THE JOURNAL OF PHYSICAL CHEMISTRY LETTERS
A JOURNAL OF THE AMERICAN CHEMICAL SOCIETY

pubs.acs.org/JPCL Letter

Ultrafast Near-Edge X-ray Absorption Fine Structure Calculations with the Exact Integral Simplified Time-Dependent Density Functional Theory (XsTD-DFT) for Large Systems

Marc de Wergifosse*

Cite This: J. Phys. Chem. Lett. 2025, 16, 13132−13138 Read Online

ACCESS | Metrics & More | Article Recommendations | Supporting Information

ABSTRACT: Computing a near-edge X-ray absorption fine structure (NEXAFS) is a real challenge for quantum chemistry (QC), as for medium to large systems, it involves a high density of core−valence excited states. With the boundaries of QC pushed at its maximum with the exact integral simplified time-dependent density functional theory (XsTD-DFT) framework, an ultrafast method is proposed to compute such excitations with short-range corrected exchange−correlation functionals using the Tamm−Dancoff approximation. For small to medium size systems, computations were performed in less than a minute, providing striking comparisons with respect to the experiment. To showcase the performance of the method, the computed oxygen K-edge NEXAFS spectrum for a collagen model of 600 atoms was compared to the experimental spectrum of collagen. Computing 85 672 $1s_O$ core−valence excited states was necessary to reproduce the experimental spectrum. The calculation took only 11 days on a desktop computer. With knowledge of the simplicity of this "small" static model of collagen, the comparison to the experiment remains excellent.

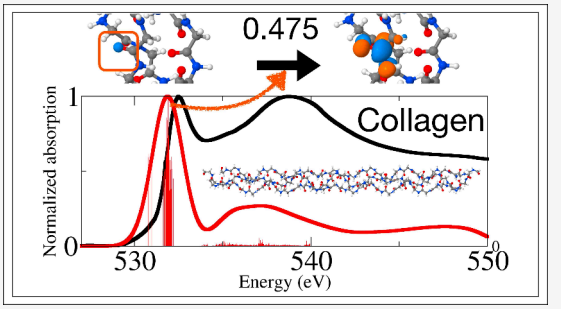

In 1913, Louis de Broglie observed for the first time the X-ray K-edge absorption spectra of bromide and silver in photographic plates, giving birth to X-ray spectroscopies.[1] With the development of synchrotron light sources,[2] the near-edge X-ray absorption fine structure (NEXAFS)[3−5] also known as the X-ray absorption fine structure (XANES) emerged as a widely used spectroscopy to characterize core−valence electronic excitations of molecules occurring below and up to 50 eV above the absorption edge[5] (e.g., K-edge). Note that, for large systems, NEXAFS spectral features are generally linked to a high density of core−valence excited states because a large number of atoms contributes to the core orbitals (e.g., 1s at C K-edge). It results that state assignments could be difficult.[5] NEXAFS measurements are now even possible with tabletop laser sources.[6] Because of these recent developments, the quantum chemistry community is under pressure to develop new theoretical tools to reproduce such experiments.[7−10] The task is not simple, as large amounts of excited states need to be computed to reach the core−valence energy window, especially for large systems. Usual methodologies employ core/valence separation (CVS),[7,11−16] also known as a restricted excitation window (REW)[8,17] in its implementation with the time-dependent density functional theory (TD-DFT).[8,18−21] The CVS approximation simply freezes most occupied orbitals that are energetically well-separated from the considered core occupied orbitals, giving rise to a small active space of occupied orbitals. For example, with the application of such an approximation to compute the carbon K-edge NEXAFS spectrum of benzene, only the six occupied 1s carbon orbitals are selected in the occupied active space. The CVS approximation is very beneficial for quantum chemistry methods to compute core−valence excitations and was applied at a plethora of levels of theory, including coupled cluster,[13,15,22−25] algebraic diagrammatic construction,[26−28] multiconfigurational,[29,30] Bethe−Salpeter equations,[31−33] and TD-DFT methods.[8−10,34] For medium-sized systems, TD-DFT is one of the main possible routes for which the CVS approximation introduces element-specific errors smaller than 1 eV for K-edge excitation energies.[35,36] Nonetheless, a large number of states might be needed to reproduce experimental energy windows, and if the system has a large density of states, the TD-DFT calculation could soon become computationally prohibitive.[10] For the interested reader, Norman and Dreuw[7] provided an excellent review on computing core excited states of molecules and Besley[8] provided another excellent one using DFT.

As discussed by Besley et al.[34] in 2009, generalized gradient approximation and hybrid exchange−correlation functionals (XCFs) usually compute strongly underestimated core−valence

Received: October 30, 2025
Revised: December 3, 2025
Accepted: December 9, 2025

https://doi.org/10.1021/acs.jpclett.5c03411
J. Phys. Chem. Lett. 2025, 16, 13132−13138

excitation energies. Long-range corrected hybrid XCFs do not improve such underestimations because they do not correct the self-interaction error at the short to middle range, which is important to correctly describe core orbitals. They argued that increasing the HF exchange at a short distance is particularly important to better treat core−valence excitations. On this basis, they introduced short-range corrected (SRC) XCFs called SRC1-R1, SRC2-R1, SRC1-R2, and SRC2-R2, specially designed to compute core−valence excitations. The SRC1 XCFs are defined as

$$E_{xc}^{\mathrm{SRC1}} = a_x E_x^{\mathrm{SR\text{-}HF}}(\omega_{\mathrm{SR}}) - a_x E_x^{\mathrm{SR\text{-}Becke}}(\omega_{\mathrm{SR}}) + b_x E_x^{\mathrm{LR\text{-}HF}}(\omega_{\mathrm{LR}}) - b_x E_x^{\mathrm{LR\text{-}Becke}}(\omega_{\mathrm{LR}}) + E_x^{\mathrm{Becke}} + E_c \quad (1)$$

while SRC2 ones adopt a different formulation

$$E_{xc}^{\mathrm{SRC2}} = a_x E_x^{\mathrm{SR\text{-}HF}}(\omega_{\mathrm{SR}}) + (1 - a_x) E_x^{\mathrm{SR\text{-}Becke}}(\omega_{\mathrm{SR}}) + b_x E_x^{\mathrm{LR\text{-}HF}}(\omega_{\mathrm{LR}}) + (1 - b_x) E_x^{\mathrm{LR\text{-}Becke}}(\omega_{\mathrm{LR}}) + E_c \quad (2)$$

These functionals are based on the splitting of the electron repulsion operator into short-range (SR) and long-range (LR) parts

$$\frac{1}{r_{12}} = \underbrace{\frac{1 - \mathrm{erf}(\omega r_{12})}{r_{12}}}_{\text{short range}} + \underbrace{\frac{\mathrm{erf}(\omega r_{12})}{r_{12}}}_{\text{long range}} \quad (3)$$

In the SRC2 XCFs that I used in this letter, a Hartree−Fock (HF) SR part scaled by a_x is included into the XCFs as well as a LR part of the HF exchange scaled by a parameter b_x. Note that, in these XCFs, the splitting parameter ω is different for the SR and LR parts. Becke exchange functional[37] at short range is scaled by $(1 - a_x)$ and at long range is scaled by $(1 - b_x)$. The correlation functional is a combination of 81% LYP[38] and 19% VWN.[39] Table 1 provides SRC2 parameters for core excitations

Table 1. Parameters Used in Both SRC2-1 and SRC2-2 XCFs

	SRC2-R1	SRC2-R2
ω_{SR}	0.69	2.20
ω_{LR}	1.02	1.80
a_x	0.55	0.91
b_x	0.08	0.28

that involve core orbitals of atoms from the first or second rows: SRC2-R1 and SRC2-R2, respectively. Note that, with SRC2-R2, higher errors on core excitation energies involving elements from the second row are expected because of missing relativistic effects.[34]

With the recent introduction of the exact integral simplified TD-DFT (XsTD-DFT) method[40−43] and its native implementation of range-separated hybrid (RSH) XCFs,[42] I adapted the method to treat core excitations of large systems and implemented SRC2 XCFs into the std2 program.[44] In the following, *i*, *j*, *k*, and *l* refer to occupied and *a*, *b*, *c*, and *d* refer to unoccupied molecular orbitals (MOs) and α, β, γ, and δ refer to atomic orbitals (AOs). Casida's equations[45] in the XsTD-DFT formalism read

$$\left[\begin{pmatrix}\mathbf{A} & \mathbf{B}\\ \mathbf{B} & \mathbf{A}\end{pmatrix} - \omega\begin{pmatrix}1 & 0\\ 0 & -1\end{pmatrix}\right]\begin{pmatrix}\mathbf{X}\\ \mathbf{Y}\end{pmatrix} = 0 \quad (4)$$

where **X** and **Y** are excitation and de-excitation vectors, respectively. Using SRC2 XCFs, XsTD-DFT **A** and **B** supermatrix elements are

$$A_{ia,jb} = \delta_{ij}\delta_{ab}(\varepsilon_a - \varepsilon_i) + 2(ia|jb)' - a_x (ij|1 - \mathrm{erf}(\omega_{\mathrm{SR}} r_{12})|ab)' - b_x (ij|\mathrm{erf}(\omega_{\mathrm{LR}} r_{12})|ab)' \quad (5)$$

and

$$B_{ia,jb} = 2(ia|bj)' - a_x (ib|1 - \mathrm{erf}(\omega_{\mathrm{SR}} r_{12})|aj)' - b_x (ib|\mathrm{erf}(\omega_{\mathrm{LR}} r_{12})|aj)' \quad (6)$$

To obtain these expressions, two simplifications were applied to TD-DFT equations. First, responses of the exchange−correlation functionals $(ia|f_{\mathrm{XC}}|jb)$ and $(ia|f_{\mathrm{XC}}|bj)$ were neglected. Second, two-electron integrals were approximated as

$$(ia|jb)' = \sum_{\alpha\beta} C_{i\alpha}^{\mathrm{low}*} C_{a\alpha}^{\mathrm{low}} C_{j\beta}^{\mathrm{low}*} C_{b\beta}^{\mathrm{low}} (\alpha\alpha|\beta\beta) \quad (7)$$

$$(ij|\mathrm{erf}(\omega_{\mathrm{LR}} r_{12})|ab)' = \sum_{\alpha\beta} Q_\alpha^{ij} Q_\beta^{ab} (\alpha\alpha|\mathrm{erf}(\omega_{\mathrm{LR}} r_{12})|\beta\beta) \quad (8)$$

and

$$(ij|1 - \mathrm{erf}(\omega_{\mathrm{SR}} r_{12})|ab)' = \sum_{\alpha\beta} Q_\alpha^{ij} Q_\beta^{ab} (\alpha\alpha|1 - \mathrm{erf}(\omega_{\mathrm{SR}} r_{12})|\beta\beta) \quad (9)$$

where Löwdin-orthogonalized coefficients $C_{\alpha i}^{\mathrm{low}}$ for each basis function α are used to determine the transition charges

$$Q_\alpha^{ia} = C_{\alpha i}^{\mathrm{low}*} C_{\alpha a}^{\mathrm{low}} \quad (10)$$

and $(\alpha\alpha|\beta\beta)$ are AO two-electron integrals in the Mulliken notation.

In the regular XsTD-DFT method,[40−43] the CI space is truncated as a function of a single energy threshold, E_{thresh}, that represents the spectral energy range. Active molecular orbitals (MOs) are selected between

$$\varepsilon_{\mathrm{min}} = \varepsilon_{\mathrm{LUMO}} - 2(1 + 0.8a_x)E_{\mathrm{thresh}} \quad (11)$$

and

$$\varepsilon_{\mathrm{max}} = \varepsilon_{\mathrm{HOMO}} + 2(1 + 0.8a_x)E_{\mathrm{thresh}} \quad (12)$$

Configuration state functions (CSFs) are sorted out if $A_{ia,ia} \leq E_{\mathrm{thresh}}$ or in the case that $A_{jb,jb} > E_{\mathrm{thresh}}$ if

$$E_{jb}^{(2)} = \sum_{ia}^{\text{P-CSFs}} \frac{|A_{ia,jb}|^2}{A_{jb,jb} - A_{ia,ia}} > 10^{-4} E_{\mathrm{h}} \quad (13)$$

The linear-response TD-DFT formalism uses a form of CVS approximation to compute core excitations, freezing all occupied orbitals except the core orbitals of interest,[8,18−21] e.g., $1s_{\mathrm{C}}$ to compute the carbon K-edge. In the selection of CSFs, the MO space is then truncated differently. The space of occupied MOs is restricted to those of interest, e.g., $1s_{\mathrm{C}}$, and the space of virtual MOs is selected based on the E_{thresh} value. In other words, among occupied orbitals, only core orbitals of interest are picked up because they are uncoupled from others and virtual MOs are selected up to

$$\varepsilon_{\mathrm{max}} = \varepsilon_{\mathrm{HOSCO}} + 2(1 + 0.8a_x)E_{\mathrm{thresh}} \quad (14)$$

https://doi.org/10.1021/acs.jpclett.5c03411
J. Phys. Chem. Lett. 2025, 16, 13132−13138

where HOSCO stands for the highest occupied selected core orbital. E_{thresh} still represents the maximum spectral range for which we would like to compute core−valence excitations. Note that, to efficiently compute **A** and **B** supermatrix elements in the truncation of the CI space for core−valence excitations using the SRC2 XCFs, CSFs are sorted out using simplified TD-DFT integrals parametrized for B3LYP (using SRC2MOs) instead of XsTD-DFT ones. Notwithstanding the fact that the B3LYP XCF underestimates core−valence excitation energies, the shape of computed NEXAFS spectra remains reasonable with respect to the experiment, showing the adequacy of the selected CSF space. The method is implemented in the std2 program.[44]

In this letter, direct comparisons to experimental K-edge NEXAFS spectra were performed to test the XsTD-DFT implementation and assess the performance of the method to compute core−valence excitations. For this, SRC XCFs (SRC2-R1 and SRC2-R2) specially designed to compute core−valence excitations as well as the core−valence cc-pCVDZ[46] basis set were used. Coronene, C_{60}, C_{70}, merocyanine, and chlorophyll A were selected as test cases from Besley[20] because of the availability of their experimental NEXAFS spectra.[47−51] To showcase the performance of the method to compute the NEXAFS spectrum of an extremely challenging system, I selected the $[(Pro\text{-}Pro\text{-}Gly)_{10}]_3$ (PPG_{10}) collagen model from de Wergifosse et al.[52] and compared it to the experimental oxygen K-edge spectrum of rat tail tendon collagen.[53] Note that PPG_{10} is composed of 600 atoms and that 15 144 primitives for a total of 2568 electrons were used for the calculations. Natural transition orbital (NTO) analysis is provided for each test cases. Computational details are provided in the Supporting Information. The Tamm−Dancoff approximation (TDA),[54] which neglects the **B** supermatrix, was used all along. All XsTDA calculations and Q-CHEM[55] SCFs were performed on a desktop computer (18 CPUs Intel Core i9-10980XE CPU at 3.00 GHz). Figure 1 depicts the optimized structures for these systems.

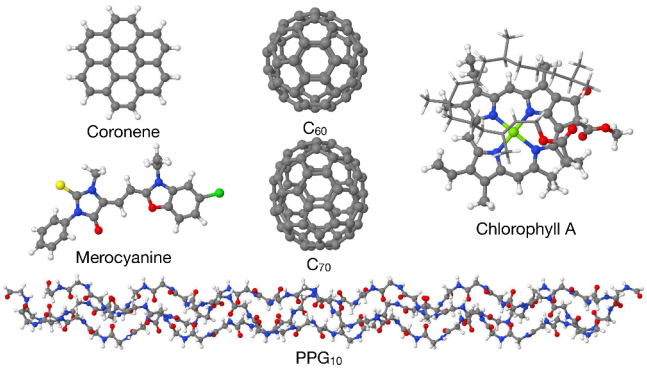

Figure 1. Optimized structures of coronene, merocyanine, C_{60}, C_{70}, chlorophyll A, and PPG_{10}.

Figure 2 presents the comparison between the experimental carbon K-edge spectrum of coronene and the computed XsSRC2/TDA and SRC2/TDA/cc-pCVDZ ones. The experimental spectrum is composed of one main absorption band with a maximum at 284.6 eV. Above 285 eV, resonant transitions are superimposed to a step-like function due to ionization processes. At higher energy, excited states have too short of a lifetime to be observed, drastically dimming down spectral features. (Xs)TDA calculations can only reproduce resonant spectral features considering an infinite lifetime for excited states. With respect to SRC2/TDA, the three first transitions computed at the XsSRC2/TDA level describing the main absorption band are shifted by −0.15, −0.17, and −0.21 eV. Both TDA and XsTDA spectra are very similar, except for higher energy core−valence excitations (>288.5 eV). Note that these electronic transitions are nonetheless badly described by such schemes due to their experimental short lifetimes. The experimental absorption maximum is 1.1 eV away from the XsTDA one located at 285.7 eV for the calculation in vacuum. With respect to the energy window, the energy shift remains small. Note that the experiment was done on a film of 300 nm deposited on copper. Thin-layer effects are totally neglected from the single static molecule calculation. Globally, the experimental spectral shape is rather well-reproduced by the XsTDA method. The most intense absorption band is split in two peaks for which three visible transitions are contributing. Figure S1 presents leading NTOs for these transitions at the XsSRC2/TDA level. The lowest visible transition located at 285.36 eV involves $1s_C$ orbitals at the edges of coronene, while the two other transitions at 285.72 and 285.80 eV involve $1s_C$ orbitals on edge carbons between C−H and the six central carbons, respectively. The SCF calculation took 112 s on 18 CPUs, while the calculation of 180 core−valence excited states took 5273 s for the TDA calculation and only 4 s for the XsTDA one. The XsTDA calculation was 1318 times faster than the TDA calculation, highlighting the extreme efficiency of the method.

Figure 2 also presents the sulfur K-edge experimental spectrum of a merocyanine dye in comparison to the XsSRC2/TDA one. While shifted by +1.2 eV with respect to the experiment, the computed XsSRC2/TDA spectrum compares very well to the experimental one. The first absorption band is composed of a unique transition at 2472.1 eV. Figure S2 illustrates the particle NTO for this transition, showing a mix of n and π^* contributions. The second computed absorption band is dominated by one transition at 2475.0 eV for which particle NTO has a d character. Note that the XsSRC2/TDA calculation took only 4 s to compute 73 $1s_S$ core−valence excitations.

Figure 3 depicts the experimental carbon K-edge NEXAFS spectra of C_{60} and C_{70} in comparison to the XsSRC2/TDA/cc-pCVDZ ones. These two very similar compounds present very distinctive NEXAFS spectra, for which the theory is able to reproduce the main differences. To illustrate these, Figures S3 and S4 present $1s_C \rightarrow \pi^*$ NTOs for the transitions dominating the two first absorption band of C_{60} and C_{70}, respectively. For these systems, the density of core−valence states increases drastically and includes a large number of degenerate states. The 1200 states of C_{60} were computed in 43 s at the XsSRC2/TDA level, while the calculation of the 1570 states of C_{70} took 35 s.

Figure 4 presents the experimental carbon K-edge NEXAFS spectrum of chlorophyll A in comparison to the XsSRC2/TDA/cc-pCVDZ one computed for its lowest energy conformer determined with the CREST procedure[56] at the GFN2-xTB[57] level of theory (see Figure 1 for its optimized structure). To compute the XsSRC2/TDA spectrum, 632 excited states were calculated in 25 s considering 3095 basis functions for 137 atoms. Here again, while the calculated spectrum is slightly shifted with respect to the experiment, the experimental shape is well-reproduced by the XsSRC2/TDA calculation. The main absorption band features two peaks composed of large numbers of transitions. This band is dominated by a transition located at 284.8 eV with an oscillator strength of 0.243 and another one at 285.6 eV with an oscillator strength of 0.546, not far from the

https://doi.org/10.1021/acs.jpclett.5c03411
J. Phys. Chem. Lett. 2025, 16, 13132−13138

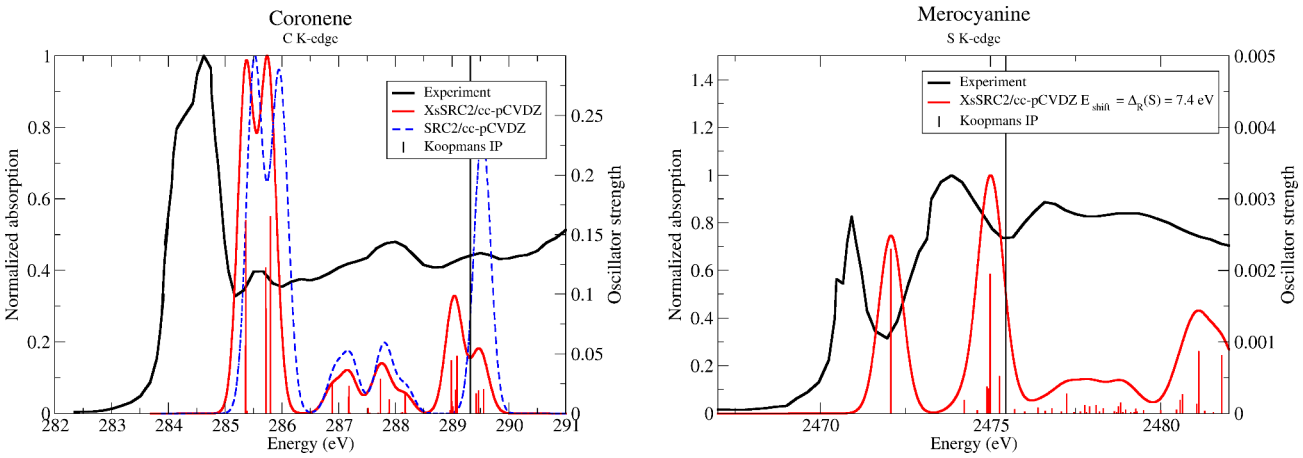

Figure 2. Experimental NEXAFS spectra of coronene (carbon K-edge, left panel)[47] and a merocyanine dye (sulfur K-edge, right panel)[50] in comparison to the XsSRC2/TDA/cc-pCVDZ ones. The SRC2/TDA/cc-pCVDZ spectrum is also included for coronene. An energy shift of $\Delta_R(S)$ = 7.4 eV was applied to merocyanine excitation energies to account for relativistic effects in the 1s core orbital of sulfur as proposed by Besley.[20] Broadening factors of 0.2 and 0.5 eV were applied, respectively.

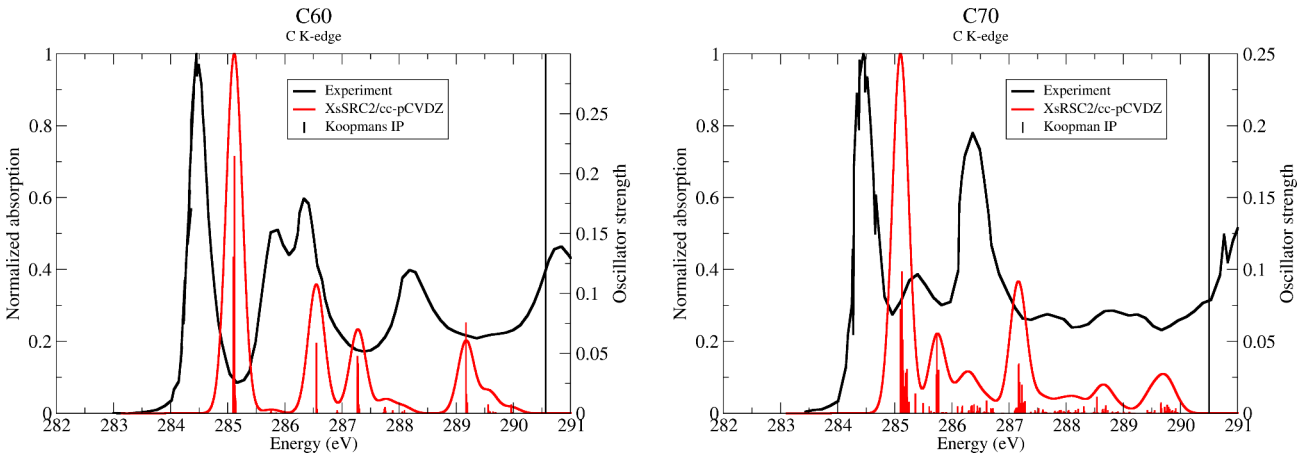

Figure 3. Experimental carbon K-edge NEXAFS spectra of C_{60} (left panel)[48] and C_{70} (right panel)[49] in comparison to the XsSRC2/TDA/cc-pCVDZ ones. A broadening factor of 0.2 eV was employed for both convoluted spectra.

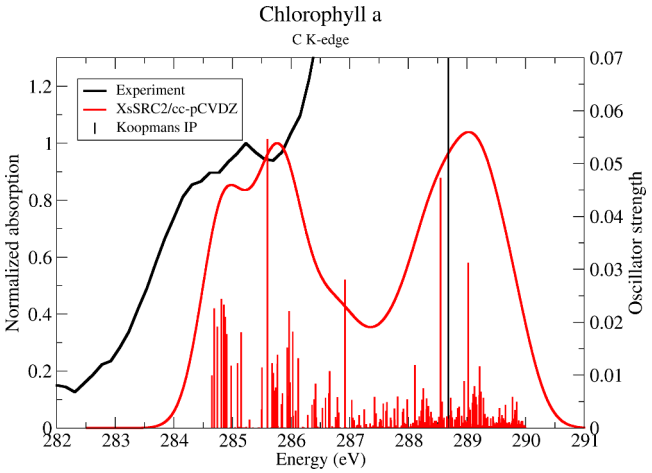

Figure 4. Experimental carbon K-edge NEXAFS spectrum of chlorophyll A[51] in comparison to the XsSRC2/TDA/cc-pCVDZ one for its lowest energy conformer. A broadening factor of 0.5 eV was employed for the convoluted spectrum.

experimental maximum of the band at 285.2 eV. Figure S5 presents NTOs related to these transitions.

Finally, to showcase the performance of the XsTDA scheme to compute $1s_O$ core−valence excitations, I selected the PPG_{10} collagen model composed of 600 atoms and computed the oxygen K-edge NEXAFS spectrum at the XsSRC2/TDA/cc-pCVDZ level of theory. A total of 85 672 excited states were computed in a little less than 11 days on my desktop computer (18 CPUs Intel Core i9-10980XE CPU at 3.00 GHz) considering an energy threshold of 550 eV. Figure 5 compares this spectrum to the experimental oxygen K-edge NEXAFS one of a collagen sample from a rat tail tendon. The experimental spectrum was recorded for a huge energy window of ∼50 eV, for which I only report the first ∼30 eV. The first absorption band is ∼5 eV wide with a maximum at 532.5 eV. Theoretically, this band is composed of 91 excitations from 530.8 to 532.3 eV. The core−valence excitation with the largest oscillator strength of 0.072 is located at 531.9 eV, only 0.6 eV away from the experimental maximum. Figure S6 depicts both leading pairs of NTOs describing this transition. In both cases, the transition occurs from $1s_O$ to a mix of n and π^* particle NTOs located on the same peptide bond. Other transitions from this absorption band are of a similar nature, for which excitation energies and strengths are modulated by their environment and positions in the chains. This "rather" sharp transition is present in all proteins

https://doi.org/10.1021/acs.jpclett.5c03411
J. Phys. Chem. Lett. 2025, 16, 13132−13138

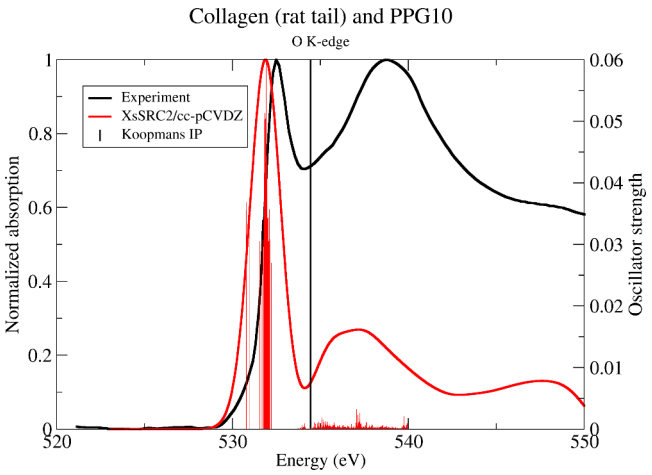

Figure 5. Experimental oxygen K-edge NEXAFS spectrum of collagen (rat tail tendon)[53] in comparison to the XsSRC2/TDA/cc-pCVDZ one for the PPG_{10} model system. A broadening factor of 1.2 eV was employed for the convoluted spectrum.

(see Figure 4 of ref 53). The second absorption band with a maximum at 538.8 eV is ∼10 eV wide. This band is more dependent on the protein[53] but is almost featureless due to short-lived excitations above the ionization threshold. A large damping parameter of 1.2 eV was used to convolute the stick spectrum and reproduce the general shape of the experimental band. The large number of transitions necessary to describe this band precludes any further analysis. The state with the largest oscillator strength is located at 537.1 eV, only 0.7 eV from the experimental maximum. All in all, with knowledge of the simplicity of this "small" static model of collagen, the comparison with respect to the experiment is excellent and pushes the boundaries of what quantum chemistry is able to do nowadays.

This letter has introduced the theoretical background to compute core−valence excitations within the XsTD-DFT framework. SRC2 XCFs were implemented as well thanks to the recent inclusion of range-separated hybrid (RSH) XCFs[42] into the std2 program.[44] Direct comparisons with respect to the experiment were performed for coronene, C_{60}, C_{70}, merocyanine, and chlorophyll A. The longest calculation took only 43 s for computing the 1200 excited states of C_{60}. While comparisons with respect to the experiment are striking, NTO analysis was also performed to characterize the nature of the excited states involved. The computed oxygen K-edge NEXAFS spectrum of the PPG_{10} collagen model was compared to the experimental one for a collagen sample to showcase the performance of the XsTDA scheme to compute core−valence excitations for a large and extremely challenging system. The calculation of 85 672 excited states took 11 days on a desktop computer. Here again, the comparison with respect to the experiment is striking. The nature of the first absorption band was analyzed with NTOs showing $1s_O$ to a mix of n and π^* characters for each peptide bonds. This new and ultrafast implementation of the XsTD-DFT scheme to compute core−valence excitations really pushes the boundaries of quantum chemistry for application to realistic systems. The next step will be to use this method in all-atom quantum mechanics (AQM) schemes[58] to account for the impact of the surroundings and dynamic structural effects to model NEXAFS spectra as it was recently proposed in my group.

■ ASSOCIATED CONTENT

Supporting Information

The Supporting Information is available free of charge at https://pubs.acs.org/doi/10.1021/acs.jpclett.5c03411.

Computational details and natural transition orbitals (PDF)

■ AUTHOR INFORMATION

Corresponding Author

Marc de Wergifosse − *Theoretical Chemistry Group, Molecular Chemistry, Materials and Catalysis Division (MOST), Institute of Condensed Matter and Nanosciences, Université Catholique de Louvain, B-1348 Louvain-la-Neuve, Belgium;* orcid.org/0000-0002-9564-7303;
Email: marc.dewergifosse@uclouvain.be

Complete contact information is available at: https://pubs.acs.org/10.1021/acs.jpclett.5c03411

Notes

The author declares no competing financial interest.

■ ACKNOWLEDGMENTS

The author thanks his Ph.D. student, Robin Crits, who performed the conformational search for chlorophyll A at the GFN2-xTB level and Prof. Benoît Champagne for his valuable comments on the manuscript.

■ REFERENCES

(1) Lamberti, C.; van Bokhoven, J. A. Introduction: Historical Perspective on XAS. In *X-ray Absorption and X-ray Emission Spectroscopy*; van Bokhoven, J. A., Lamberti, C., Eds.; John Wiley & Sons, Ltd.: Hoboken, NJ, 2016; Chapter 1, pp 1−21, DOI: 10.1002/9781118844243.ch1.

(2) Robinson, A. L. History of Synchrotron Radiation. *Synchrotron Radiat. News* **2015**, *28*, 4−9.

(3) Stöhr, J. *NEXAFS Spectroscopy*; Springer Science & Business Media: Berlin, Germany, 2013; Vol. *25*.

(4) Rehr, J. J.; Albers, R. C. Theoretical Approaches to X-ray Absorption Fine Structure. *Rev. Mod. Phys.* **2000**, *72*, 621−654.

(5) Hähner, G. Near Edge X-ray Absorption Fine Structure Spectroscopy as a Tool to Probe Electronic and Structural Properties of Thin Organic Films and Liquids. *Chem. Soc. Rev.* **2006**, *35*, 1244−1255.

(6) Depresseux, A.; et al. Table-top Femtosecond Soft X-ray Laser by Collisional Ionization Gating. *Nat. Phot.* **2015**, *9*, 817−821.

(7) Norman, P.; Dreuw, A. Simulating X-ray Spectroscopies and Calculating Core-Excited States of Molecules. *Chem. Rev.* **2018**, *118*, 7208−7248.

(8) Besley, N. A. Modeling of the Spectroscopy of Core Electrons with Density Functional Theory. *WIREs Comp. Mol. Sci.* **2021**, *11*, e1527.

(9) Nascimento, D. R.; Govind, N. Computational Approaches for XANES, VtC-XES, and RIXS using Linear-Response Time-Dependent Density Functional Theory Based Methods. *Phys. Chem. Chem. Phys.* **2022**, *24*, 14680−14691.

(10) Herbert, J. M.; Zhu, Y.; Alam, B.; Ojha, A. K. Time-Dependent Density Functional Theory for X-ray Absorption Spectra: Comparing the Real-Time Approach to Linear Response. *J. Chem. Theory Comput.* **2023**, *19*, 6745−6760.

(11) Cederbaum, L. S.; Domcke, W.; Schirmer, J. Many-Body Theory of Core Holes. *Phys. Rev. A* **1980**, *22*, 206−222.

(12) Barth, A.; Cederbaum, L. S. Many-Body Theory of Core-Valence Excitations. *Phys. Rev. A* **1981**, *23*, 1038−1061.

(13) Coriani, S.; Koch, H. Communication: X-ray Absorption Spectra and Core-Ionization Potentials within a Core-Valence Separated Coupled Cluster Framework. *J. Chem. Phys.* **2015**, *143*, 181103.

(14) Wenzel, J.; Holzer, A.; Wormit, M.; Dreuw, A. Analysis and Comparison of CVS-ADC Approaches up to Third Order for the Calculation of Core-Excited States. *J. Chem. Phys.* **2015**, *142*, 214104.
(15) Vidal, M. L.; Feng, X.; Epifanovsky, E.; Krylov, A. I.; Coriani, S. New and Efficient Equation-of-Motion Coupled-Cluster Framework for Core-Excited and Core-Ionized States. *J. Chem. Theory Comput.* **2019**, *15*, 3117−3133.
(16) Mazin, I. M.; Sokolov, A. Y. Core-Excited States and X-ray Absorption Spectra from Multireference Algebraic Diagrammatic Construction Theory. *J. Chem. Theory Comput.* **2023**, *19*, 4991−5006.
(17) Bussy, A.; Hutter, J. Efficient and Low-Scaling Linear-Response Time-Dependent Density Functional Theory Implementation for Core-Level Spectroscopy of Large and Periodic Systems. *Phys. Chem. Chem. Phys.* **2021**, *23*, 4736−4746.
(18) Stener, M.; Fronzoni, G.; de Simone, M. Time Dependent Density Functional Theory of Core Electrons Excitations. *Chem. Phys. Lett.* **2003**, *373*, 115−123.
(19) Lestrange, P. J.; Nguyen, P. D.; Li, X. Calibration of Energy-Specific TDDFT for Modeling K-edge XAS Spectra of Light Elements. *J. Chem. Theory Comput.* **2015**, *11*, 2994−2999.
(20) Besley, N. A. Fast Time-Dependent Density Functional Theory Calculations of the X-ray Absorption Spectroscopy of Large Systems. *J. Chem. Theory Comput.* **2016**, *12*, 5018−5025.
(21) Hanson-Heine, M. W. D.; George, M. W.; Besley, N. A. Assessment of Time-Dependent Density Functional Theory with the Restricted Excitation Space Approximation for Excited State Calculations of Large Systems. *Mol. Phys.* **2018**, *116*, 1452−1459.
(22) Coriani, S.; Christiansen, O.; Fransson, T.; Norman, P. Coupled-Cluster Response Theory for Near-Edge X-ray-Absorption Fine Structure of Atoms and Molecules. *Phys. Rev. A* **2012**, *85*, 022507.
(23) Fransson, T.; Coriani, S.; Christiansen, O.; Norman, P. Carbon X-ray Absorption Spectra of Fluoroethenes and Acetone: A Study at the Coupled Cluster, Density Functional, and Static-Exchange Levels of Theory. *J. Chem. Phys.* **2013**, *138*, 124311.
(24) Nascimento, D. R.; DePrince, A. E. I. Simulation of Near-Edge X-ray Absorption Fine Structure with Time-Dependent Equation-of-Motion Coupled-Cluster Theory. *J. Phys. Chem. Lett.* **2017**, *8*, 2951−2957.
(25) Park, Y. C.; Perera, A.; Bartlett, R. J. Equation of Motion Coupled-Cluster Study of Core Excitation Spectra II: Beyond the Dipole Approximation. *J. Chem. Phys.* **2021**, *155*, 094103.
(26) Wenzel, J.; Wormit, M.; Dreuw, A. Calculating Core-Level Excitations and X-ray Absorption Spectra of Medium-Sized Closed-Shell Molecules with the Algebraic-Diagrammatic Construction Scheme for the Polarization Propagator. *J. Comput. Chem.* **2014**, *35*, 1900−1915.
(27) Wenzel, J.; Wormit, M.; Dreuw, A. Calculating X-ray Absorption Spectra of Open-Shell Molecules with the Unrestricted Algebraic-Diagrammatic Construction Scheme for the Polarization Propagator. *J. Chem. Theory Comput.* **2014**, *10*, 4583−4598.
(28) Wenzel, J.; Holzer, A.; Wormit, M.; Dreuw, A. Analysis and Comparison of CVS-ADC Approaches up to Third Order for the Calculation of Core-Excited States. *J. Chem. Phys.* **2015**, *142*, 214104.
(29) Josefsson, I.; Kunnus, K.; Schreck, S.; Föhlisch, A.; de Groot, F.; Wernet, P.; Odelius, M. Ab Initio Calculations of X-ray Spectra: Atomic Multiplet and Molecular Orbital Effects in a Multiconfigurational SCF Approach to the L-Edge Spectra of Transition Metal Complexes. *J. Phys. Chem. Lett.* **2012**, *3*, 3565−3570.
(30) Pinjari, R. V.; Delcey, M. G.; Guo, M.; Odelius, M.; Lundberg, M. Restricted Active Space Calculations of L-Edge X-ray Absorption Spectra: From Molecular Orbitals to Multiplet States. *J. Chem. Phys.* **2014**, *141*, 124116.
(31) Onida, G.; Reining, L.; Rubio, A. Electronic Excitations: Density-Functional versus Many-Body Green's-Function Approaches. *Rev. Mod. Phys.* **2002**, *74*, 601−659.
(32) Vinson, J.; Rehr, J. J.; Kas, J. J.; Shirley, E. L. Bethe-Salpeter Equation Calculations of Core Excitation Spectra. *Phys. Rev. B* **2011**, *83*, 115106.
(33) Yao, Y.; Golze, D.; Rinke, P.; Blum, V.; Kanai, Y. All-Electron BSE@GW Method for K-Edge Core Electron Excitation Energies. *J. Chem. Theory Comput.* **2022**, *18*, 1569−1583.
(34) Besley, N. A.; Peach, M. J. G.; Tozer, D. J. Time-Dependent Density Functional Theory Calculations of Near-Edge X-ray Absorption Fine Structure with Short-Range Corrected Functionals. *Phys. Chem. Chem. Phys.* **2009**, *11*, 10350−10358.
(35) Herbst, M. F.; Fransson, T. Quantifying the Error of the Core−Valence Separation Approximation. *J. Chem. Phys.* **2020**, *153*, 054114.
(36) Helmich-Paris, B. Simulating X-ray Absorption Spectra with Complete Active Space Self-Consistent Field Linear Response Methods. *Int. J. Quantum Chem.* **2021**, *121*, e26559.
(37) Becke, A. D. Density-Functional Exchange-Energy Approximation with Correct Asymptotic Behavior. *Phys. Rev. A* **1988**, *38*, 3098−3100.
(38) Lee, C.; Yang, W.; Parr, R. G. Development of the Colle-Salvetti Correlation-Energy Formula into a Functional of the Electron Density. *Phys. Rev. B* **1988**, *37*, 785−789.
(39) Vosko, S. H.; Wilk, L.; Nusair, M. Accurate Spin-Dependent Electron Liquid Correlation Energies for Local Spin Density Calculations: a Critical Analysis. *Can. J. Phys.* **1980**, *58*, 1200−1211.
(40) Löffelsender, S.; Beaujean, P.; de Wergifosse, M. Simplified Quantum Chemistry Methods to Evaluate Non-Linear Optical Properties of Large Systems. *WIREs Comp. Mol. Sci.* **2024**, *14*, e1695.
(41) de Wergifosse, M.; Grimme, S. The eXact Integral Simplified Time-Dependent Density Functional Theory (XsTD-DFT). *J. Chem. Phys.* **2024**, *160*, 204110.
(42) de Wergifosse, M. Computing Excited States of Very Large Systems with Range-Separated Hybrid Functionals and the eXact Integral Simplified Time-Dependent Density Functional Theory (XsTD-DFT). *J. Phys. Chem. Lett.* **2024**, *15*, 12628−12635.
(43) Maraldi, M. G.; de Wergifosse, M. Evaluating the Performance of the Exact Integral Simplified Time-Dependent Density Functional Theory (XsTD-DFT) to Compute One- and Two-Photon Absorption. *J. Phys. Chem. A* **2025**, *129*, 8178−8203.
(44) *std2 (Version 2.0.1): A Program for Computing Excited States and Response Functions via Simplified TD-DFT Methods (sTDA, sTD-DFT, SF-sTD-DFT, XsTDA, XsTD-DFT, and SF-Xs-TD-DFT)*, 2025; DOI: 10.5281/zenodo.14849828.
(45) Casida, M. E. Time-Dependent Density Functional Response Theory for Molecules. *Recent Advances in Density Functional Methods* **1995**, *1*, 155−192.
(46) Woon, D. E.; Dunning, T. H. Gaussian Basis Sets for Use in Correlated Molecular Calculations. V. Core-Valence Basis Sets for Boron Through Neon. *J. Chem. Phys.* **1995**, *103*, 4572−4585.
(47) Oji, H.; Mitsumoto, R.; Ito, E.; Ishii, H.; Ouchi, Y.; Seki, K.; Yokoyama, T.; Ohta, T.; Kosugi, N. Core Hole Effect in NEXAFS Spectroscopy of Polycyclic Aromatic Hydrocarbons: Benzene, Chrysene, Perylene, and Coronene. *J. Chem. Phys.* **1998**, *109*, 10409−10418.
(48) Luo, Y.; Ågren, H.; Gel'mukhanov, F.; Guo, J.; Skytt, P.; Wassdahl, N.; Nordgren, J. Symmetry-Selective Resonant Inelastic X-ray Scattering of C_{60}. *Phys. Rev. B* **1995**, *52*, 14479−14496.
(49) Guo, J.; Skytt, P.; Wassdahl, N.; Nordgren, J.; Luo, Y.; Vahtras, O.; Ågren, H. Resonant and Non-Resonant X-ray Scattering from C70. *Chem. Phys. Lett.* **1995**, *235*, 152−159.
(50) Smith, T. A.; DeWitt, J. G.; Hedman, B.; Hodgson, K. O. Sulfur and Chlorine K-Edge X-ray Absorption Spectroscopic Studies of Photographic Materials. *J. Am. Chem. Soc.* **1994**, *116*, 3836−3847.
(51) Legall, H.; Stiel, H.; Beck, M.; Leupold, D.; Gruszecki, W. I.; Lokstein, H. Near Edge X-ray Absorption Fine Structure Spectroscopy (NEXAFS) of Pigment-Protein Complexes: Peridinin-Chlorophyll a Protein (PCP) of Amphidinium Carterae. *J. Biochem. Biophys. Methods* **2007**, *70*, 369−376.
(52) de Wergifosse, M.; de Ruyck, J.; Champagne, B. How the Second-Order Nonlinear Optical Response of the Collagen Triple Helix Appears: A Theoretical Investigation. *J. Phys. Chem. C* **2014**, *118*, 8595−8602.

(53) Zubavichus, Y.; Shaporenko, A.; Grunze, M.; Zharnikov, M. NEXAFS Spectroscopy of Biological Molecules: From Amino Acids to Functional Proteins. *NIM-A or Nucl. Instrum. Methods Phys. Res. A* **2009**, *603*, 111−114.
(54) Hirata, S.; Head-Gordon, M. Time-Dependent Density Functional Theory Within the Tamm-Dancoff Approximation. *Chem. Phys. Lett.* **1999**, *314*, 291−299.
(55) Epifanovsky, E.; et al. Software for the Frontiers of Quantum Chemistry: An Overview of Developments in the Q-Chem 5 Package. *J. Chem. Phys.* **2021**, *155*, 084801.
(56) Pracht, P.; Bohle, F.; Grimme, S. Automated Exploration of the Low-Energy Chemical Space with Fast Quantum Chemical Methods. *Phys. Chem. Chem. Phys.* **2020**, *22*, 7169−7192.
(57) Bannwarth, C.; Ehlert, S.; Grimme, S. GFN2-XTB—An Accurate and Broadly Parametrized Self-Consistent Tight-Binding Quantum Chemical Method with Multipole Electrostatics and Density-Dependent Dispersion Contributions. *J. Chem. Theory Comput.* **2019**, *15*, 1652−1671.
(58) Löffelsender, S.; Maraldi, M. G.; de Wergifosse, M. All-Atom Quantum Mechanical (AQM) Methodologies to Evaluate One- and Two-Photon Absorption of Realistic Systems. *ChemPhysChem* **2025**, *26*, e202401121.

https://doi.org/10.1021/acs.jpclett.5c03411
J. Phys. Chem. Lett. 2025, 16, 13132−13138